

Selective excitation of quantum wave packets in a classical chaotic environment

P. A. Braun and V. I. Savichev

St. Petersburg Institute of Nuclear Physics (B. P. Konstantinov), Russian Academy of Sciences, 188350

St. Petersburg, Russia

(Submitted 24 March 1995)

Zh. Éksp. Teor. Fiz. **108**, 464–484 (August 1995)

We examine the preparation and temporal evolution of quantum wave packets from Rydberg states of a hydrogen atom in a magnetic field; the energy range corresponds to classical chaotic dynamics. Excitation via an intermediate state of the regular Rydberg spectrum results in a significant simplification of the spectrum of oscillator strengths, and the production of wave packets that evolve along selected closed classical trajectories. © 1995 American Institute of Physics.

1. INTRODUCTION

The temporal evolution of Rydberg wave packets has recently come under close theoretical and experimental scrutiny.¹ A Rydberg wave packet consists of a superposition of high-excitation states that have been coherently populated by a brief laser pulse. It evolves in both space and time, and mimics the motion of a classical particle. One of the most important outcomes of such studies is that they afford clarification of fundamental questions about the correspondence between classical and quantum mechanics.

Two typical situations have been addressed in studies of Rydberg wave packets thus far. In the first, the wave packet is excited in a minimally anharmonic region of the regular spectrum;² a familiar feature seen in the temporal evolution of this sort of wave packet is a regular sequence of decays and revivals.^{3–5} In the second, an atom initially in its ground state produces a packet of states near the ionization threshold, close to the corresponding chaotic regime of classical dynamics.¹ In the latter case, the salient characteristics of the packet's temporal evolution are linked to the existence of closed classical trajectories that originate and terminate on the nucleus.^{6,7} Ordinarily, many such trajectories can be excited from the ground state, and the evolution of the packet is fairly complicated.

Bouloufa *et al.*⁸ recently advanced the idea of selective excitation of Rydberg states in the irregular part of the spectrum. Selectivity results from excitation via an intermediate Rydberg state of the regular spectrum, making it possible to enhance the contribution of some chosen classical trajectory.⁹

Our objective here is to make use of the selective excitation concept in order to produce wave packets in the irregular part of the quantum spectrum. The quantum system considered is a hydrogen atom in a magnetic field, and we use one of the odd states of the diamagnetic multiplet as the Rydberg state of the regular spectrum.

Atomic units are employed throughout, with $\hbar = e = m = 1$.

2. HYDROGEN ATOM IN A MAGNETIC FIELD

The nonrelativistic Hamiltonian of a hydrogen atom in a magnetic field \mathbf{B} that points in the z direction is

$$H = \frac{\mathbf{p}^2}{2} - \frac{1}{r} + \frac{\gamma}{2} L_z + \frac{\gamma^2}{8} \rho^2, \quad (1)$$

where $\rho^2 = x^2 + y^2$ and $\gamma = B/B_c$ ($B_c = 2.35 \cdot 10^5 T$). In the nonrelativistic approximation, $\gamma L_z/2$ is a constant of the motion, and is equal to $\gamma m/2$. Henceforth we only consider states with $m = 0$.

2.1. Weak-field limit (I -mixing regime)

The operator $\gamma^2 \rho^2/8$ leads to diamagnetic splitting. If the splitting is much smaller than the separation between degenerate hydrogen levels that differ in n , i.e.,

$$\gamma^2 n^4 \ll 1/n^3, \quad (2)$$

the proper zeroth-order wave function will be

$$|\psi\rangle = \sum_{l=|m|}^{n-1} C_l |nlm\rangle. \quad (3)$$

In first-order perturbation theory, the energy levels will be $E = E^{(0)} + E^{(d)}$, where $E^{(0)} = -1/(2n^2)$ and the $E^{(d)}$ are the eigenvalues of the matrix

$$V_{ll'} = \frac{\gamma^2}{8} \langle nlm | \rho^2 | nl'm \rangle. \quad (4)$$

All states have either even or odd parity, given by $(-1)^{K+m}$, where K is the quantum number that labels the vertex of the multiplet, $K = 0, \dots, n - |m| - 1$.

From the standpoint of classical mechanics, the presence of a weak magnetic field will lead to a slow alteration in the shape and orientation of the Keplerian ellipse. The orbit's semimajor axis oscillates near the direction of the field vector or near the xy plane. These two possibilities correspond to vibrational and rotational motion, respectively. Vibrational motion occurs in quantum states in the lower part of a diamagnetic multiplet, while rotational motion occurs in the upper part. At maximum inclination of the semimajor axis of the ellipse, the electron's angular momentum \mathbf{L} vanishes and the ellipse degenerates into a straight line. For a state with energy $E^{(d)}$, the maximum inclination is given by

$$\sin^2 \theta_0 = \frac{16E^{(d)}}{5n^4 \gamma^2}. \quad (5)$$

This angle plays the role of the turning point in oscillations of the semimajor axis of a classical orbit. In the quantum problem, the angle θ_0 locates the maximum in the angular distribution of probability density for a diamagnetic state of energy $E^{(d)}$.⁹ The lowest vibrational state corresponds to $\theta_0 \approx 0$, and the highest rotational state to $\theta_0 \approx 90^\circ$.

The angle θ_0 plays an important role in an examination of optical transitions between sublevels of two different diamagnetic Rydberg multiplets. In a classical setting, a Rydberg electron absorbs and emits light most intensely when its acceleration is greatest. This occurs when the electron comes closest to the nucleus, i.e., when the electron's orbit degenerates into a straight line passing through the nucleus and making an angle θ_0 with the magnetic field. The present discussion applies both to the lower and upper diamagnetic Rydberg state.

Since θ_0 is a turning point, and therefore represents a maximum in the probability density, we expect that the most likely of all feasible transitions between sublevels of two high-excitation shells are the ones for which these maxima overlap, i.e., for which θ_0 has the same value in the initial and final state. This has been borne out by numerical calculations.⁹ Hence, we have a distinctive Franck–Condon principle for optical transitions between perturbed Rydberg sublevels: transitions occur principally when the classical orbit passes through the nucleus, with the velocity of the Rydberg electron at the time of passage changing in magnitude but not direction.

2.2. Strong-field limit (n -mixing regime)

Closer to the ionization limit, diamagnetic multiplets start to cross. Accurate calculation of the quantum spectrum and wave functions in the n -mixing regime requires that we numerically diagonalize the Hamiltonian (1) in some suitable basis. Appendix A provides a brief description of the algorithm used here.

The main result is that the spectrum turns out to be quite complicated. The irregular nature of the spectrum mirrors the onset of chaos in the corresponding classical problem. Periodic and closed classical trajectories play a major role in the semiclassical approach to calculating irregular quantum spectra.^{6,7,10,11}

Consider an optical transition from a lower state located somewhere in the discrete spectrum. Since the initial state is typically much smaller than the excited states of the irregular spectrum, closed classical trajectories that pass through the nucleus are the most prominent contributors. The oscillator-strength density, defined as the sum over all final upper states,

$$f(E) = \sum_s \delta(E - E_s) f_s, \quad (6)$$

where E_s and f_s are the energy of the upper state and the corresponding transition oscillator strength (the absolute square of the dipole matrix element), is given in the semiclassical limit¹⁾ by^{6,7}

$$f(E) = f_0(E) + N \sum_j \frac{A^*(\theta_j^f) A(\theta_j^i)}{\sqrt{|M_{12}^{(j)}|}} \sin\left(\frac{S_j}{\hbar} - \nu_j \frac{\pi}{2}\right), \quad (7)$$

where E is the energy in the irregular part of the spectrum; the sum is taken over all closed classical trajectories (including repetitions); $f_0(E)$ is a smooth function of the energy; N is a constant; $M_{12}^{(j)}$ is a matrix element of the monodromy matrix; ν_j is the Maslov index of a given classical trajectory; $A(\theta)$ is the angular distribution function for outgoing waves when a photon is absorbed by an electron near the nucleus; and θ_j^i and θ_j^f are the initial and final polar angles of a classical trajectory that traverses the nucleus. For a linearly polarized laser pulse, the angular distribution is

$$A(\theta) = \sqrt{\sin \theta} \sum_{l'} (-1)^{l'} \langle \psi | z | [n_{\text{eff}}] l' m \rangle Y_{l' m}(\theta, 0), \quad (8)$$

where $|\psi\rangle$ is the wave function of the lower diamagnetic state, and $|[n_{\text{eff}}] l m\rangle$ is the hydrogen wave function with principal quantum number equal to the integer part of $n_{\text{eff}} = 1/\sqrt{-2E}$.

The semiclassical expressions (7) and (8) hold for classical trajectories with $\theta^f, \theta^i \neq 0$. The modification for a classical trajectory linear in the field is given in Appendix B; for $A(\theta)$, it makes the factor $\sqrt{\sin \theta}$ in Eq. (8) vanish.

We now assume that the Franck–Condon principle also holds for transitions to states of the irregular spectrum—in other words, that immediately after a transition, the angle θ_0 between the velocity of a classical electron and the magnetic field is determined by the lower (regular) state. In the expansion (7), we then expect the greatest contribution to come from classical orbits with initial angles (between the field and the electron velocity upon emergence of the electron from the nucleus) close to θ_0 . This is confirmed by the calculations: the semiclassical angular distribution function $|A(\theta)|^2$ computed for transitions from some lower l -mixed diamagnetic state $|\psi\rangle$ does in fact have a maximum near the corresponding angle of maximum deviation of the semimajor axis θ_0 .

In somewhat simplified terms, we may say that excitation from the various states of a diamagnetic multiplet selectively populates states of the irregular spectrum that are reasonably well localized along some closed classical trajectory. The polar angle at which the given trajectory exits the nucleus must equal θ_0 , the maximum deviation of the semimajor axis in the initial diamagnetic state [see Eq. (5)].

2.3. Closed classical trajectories in the chaotic regime

The classical problem of a hydrogen atom in a magnetic field can, by a scaling transformation, be reduced to a problem that depends solely on the parameter¹²

$$\varepsilon = E \gamma^{-2/3}. \quad (9)$$

The limit $\varepsilon \rightarrow -\infty$ corresponds exactly to the integrable Coulomb problem. When $\varepsilon \ll -1$, classical perturbation theory in a weak magnetic field applies. As ε increases, the chaotic component starts to fill phase space, and islands of regular motion concentrate about stable periodic orbits.¹² The most

important of these are the shortest-period closed classical trajectories,²⁾ which are rectilinear trajectories along (I_∞) and across (I_1) the field.

Consider the evolution of I_∞ and I_1 orbits as ε increases. A bifurcation takes place at $\varepsilon \approx -0.39$, whereupon the I_∞ trajectory becomes unstable and a new stable closed trajectory I_2 is born. At $\varepsilon \approx -0.33$, I_∞ becomes stable and a new unstable trajectory is born. As we pass to the ionization limit $\varepsilon = 0$, I_∞ undergoes an infinite series of like bifurcations.¹³ The trajectory I_2 becomes unstable at $\varepsilon \approx -0.29$, accompanied by the birth of a periodic trajectory that does not pass through the nucleus. I_1 remains stable down to $\varepsilon \approx -0.13$.

Note that the bifurcations described above are accompanied by the emergence of new classical trajectories with the same period and action as the original one. The bifurcation of multiply periodic classical orbits is described by Holle *et al.*¹⁴

3. EXCITATION BY A SHORT LASER PULSE

Following excitation by a short Gaussian laser pulse linearly polarized along the field, we obtain to first order in time-dependent perturbation theory the wave packet

$$|t\rangle = \frac{1}{N} \sum_s B_s |s\rangle \exp(-iE_s t), \quad (10)$$

where E_s and $|s\rangle$ are eigenvalues and eigenfunctions of the Hamiltonian (1); N is a normalizing constant; the expansion coefficients are

$$B_s = \exp[-(E_s - \omega)^2 \tau_p^2] \langle s|z|\psi\rangle, \quad (11)$$

and $\langle s|z|\psi\rangle$ is the dipole matrix element from the upper state.

For $|\psi\rangle$ we select one of the odd states of the quadratic Zeeman multiplet with $n=20$, $m=0$; the upper states $|s\rangle$ belong to the irregular part of the spectrum, and correspond to energies $E \equiv -1/(2n_{\text{eff}}^2)$, with $n_{\text{eff}} \approx 90$.

3.1. Excitation of the orbit I_∞

We see from the foregoing considerations that to excite states of the irregular spectrum localized along a linear trajectory I_∞ pointing in the direction of the field, we must choose the initial state to be the lowest-lying vibrational state with $K=19$ for which the corresponding classical angle of maximum deviation of the semimajor axis is close to zero. The angular distribution function (8) corresponding to this case is shown in Fig. 1 (to calculate curve 1, we used $A(\theta)$ for a linear trajectory directed along the field).

The oscillator-strength spectrum in the region corresponding to the reduced energy $\varepsilon = -0.5$ is shown in Fig. 2. It is obviously exceedingly regular, and its most important features can be explained in very simple terms. The main sequence of lines gives rise to a Coulomb series of levels:

$$E_n = -\frac{1}{2[n + \Delta(n)]^2}, \quad \Delta(n+1) - \Delta(n) \ll 1. \quad (12)$$

This can easily be accounted for if we assume that these levels correspond to the states most heavily localized along the field. According to (1), such states are virtually unaf-

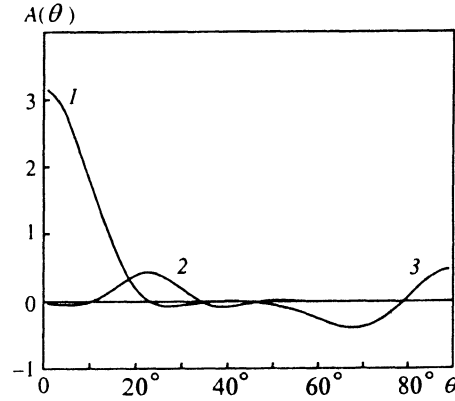


FIG. 1. Angular distribution function $A(\theta)$. Excitation from lower diamagnetic states with 1) $K=19$; 2) $K=15$; 3) $K=1$.

ected by the magnetic field, and are essentially Rydberg Coulomb states. Regular satellite lines are also visible in Fig. 2, corresponding to quantization in the plane perpendicular to the given classical trajectory.

To illustrate the nature of the selectivity, we show in Fig. 3 the oscillator-strength spectrum for a "nonselective" excitation out of the $2p$ state. This spectrum is much more complicated, and the strongest contribution (main sequence) comes from states localized in the xy plane, i.e., associated entirely with the other classical orbit I_1 .

The dashed curve in Fig. 2 is the pulse envelope, with an effective wave-packet width of $\Delta n \approx 6$. Useful quantities characterizing the temporal dynamics of the wave packet include the correlation function

$$|\langle 0|t\rangle|^2 = \frac{1}{N^4} \sum_{s,s'} B_s^2 B_{s'}^2 \exp[-i(E_{s'} - E_s)t] \quad (13)$$

and the time-dependence of the expectation values of various physical observables \hat{A} in the packet state, i.e.,

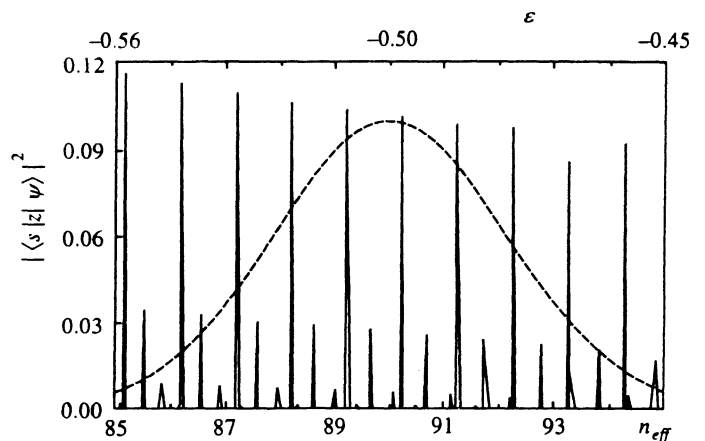


FIG. 2. Spectrum of oscillator strengths $|\langle s|z|\psi\rangle|^2$ upon excitation from a lower diamagnetic state with $K=19$ in the energy range corresponding to $\varepsilon = -0.5$, with $n_{\text{eff}} = \sqrt{-2E}$.

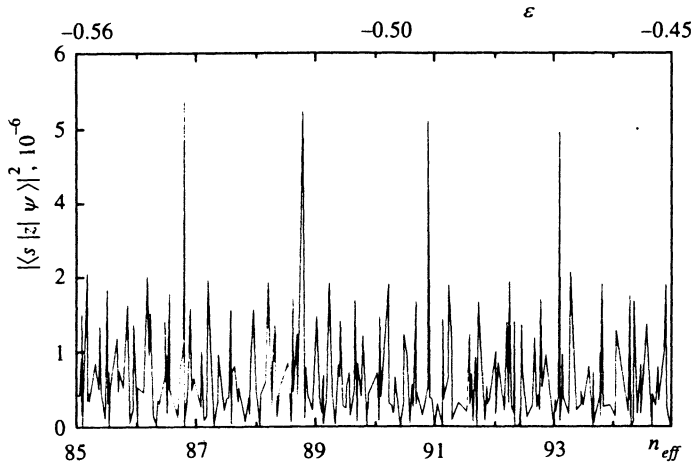


FIG. 3. Spectrum of oscillator strengths upon excitation from the 2p state.

$$\langle t|\hat{A}|t\rangle = \sum_{s,s'} B_s^* B_{s'} \langle s|\hat{A}|s'\rangle \exp[-i(E_{s'} - E_s)t]. \quad (14)$$

The correlation function indicates the extent to which the initial state is reproduced, while the packet means, according to the correspondence principle, are related to the temporal evolution of the corresponding classical quantities. For the latter, we will be concerned with z^2 and ρ^2 .

Figure 4 shows the evolution of the correlation function as a function of the rescaled time t/T_{cl} , where

$$T_{cl} = \frac{2\pi}{\Delta E} \approx 2\pi n_{eff}^3 \quad (15)$$

is the Coulomb period, which is the same as the orbital period of I_∞ . In this plot we see oscillations at the classical period T_{cl} modulated in amplitude by a process that corresponds to motion along the classical trajectory, with alternating decay and revival of the wave packet. In among the oscillations at the fundamental classical frequency are faster oscillations at higher frequencies.

Features such as these find a natural explanation in the quasi-one-dimensional evolution of a wave packet whose spectrum displays weak anharmonicity.^{3,4} The natural "one-dimensionalization" factor in the full two-dimensional prob-

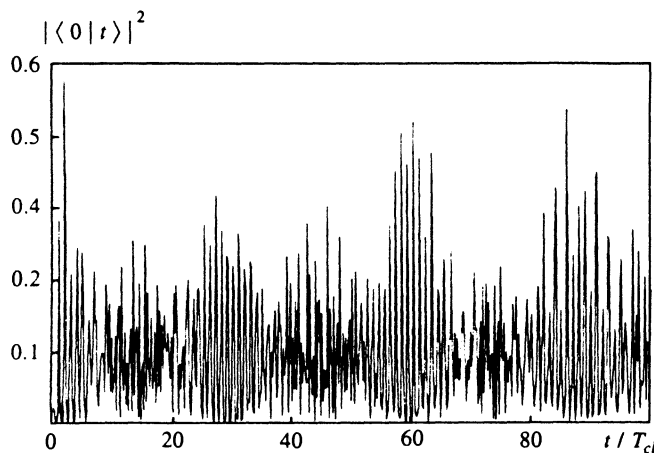


FIG. 4. Time dependence of the correlation function; $K = 19$, $\varepsilon = -0.5$.

lem is the strong localization of the wave packet along the classical trajectory I_∞ . By way of illustration, Fig. 5 shows surface plots of the evolution of the probability density over the time interval $[0, T_{cl}]$.

Let us briefly recall the basic features of wave packet evolution for packets prepared in a regular spectral region with weak anharmonicity. The energy levels in that region can be written in the form

$$E_n - E_{n_0} \approx \omega(n - n_0) + \lambda(n - n_0)^2 + \gamma(n - n_0)^3 + \delta(n - n_0)^4 + \dots, \quad (16)$$

$$\omega \gg \lambda \gg \gamma \gg \delta.$$

We now substitute (16) into (10). At times of order $1/\omega$, we can neglect the contribution of all but the linear term to the phase of the wave functions in the packet (10). This leads to periodic oscillations at the classical period $T_{cl} = 2\pi/\omega$, which corresponds to packet motion along the classical trajectory. At $t \gg T_{cl}$, the nonvanishing anharmonicity λ results in dephasing, with a subsequent series of decays and revivals of the wave packet at a period

$$T_{rev} = \pi/\lambda. \quad (17)$$

In fact, at time $t \approx T_{rev}$, the quadratic anharmonicity leads to recovery of the original packet, shifted in time by $T_{cl}/2$:

$$|t\rangle \approx |t + T_{cl}/2\rangle_{in}, \quad (18)$$

where

$$|t\rangle_{in} = \frac{1}{N} \sum_s B_s |s\rangle \exp(-i\omega s t)$$

is the wave packet with no allowance for anharmonic corrections to the spectrum.

Furthermore, there exist so-called fractional-order revivals at times $T_{rev}/2$, $T_{rev}/3$, etc., which are related to fragmentation of the wave packet. In a plot showing temporal evolution, these correspond to oscillations at frequencies 2ω , 3ω , etc.³

To calculate the revival period in the present instance, we note that λ , according to (12), takes the form

$$\lambda = \frac{3}{2n_0^4} \left(1 + \frac{d\Delta(n_0)}{dn} \right). \quad (19)$$

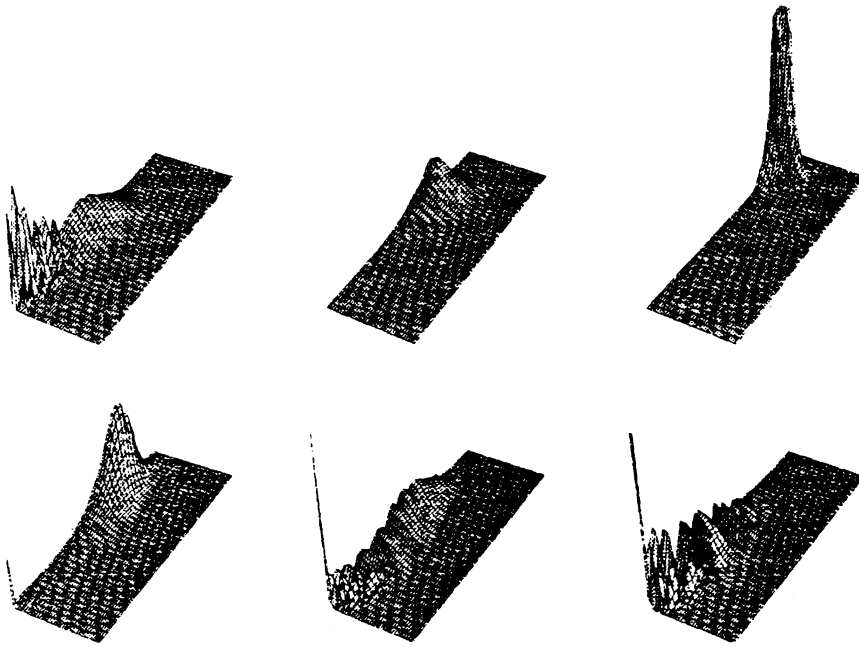


FIG. 5. Evolution of the probability density for a wave packet corresponding to the classical trajectory I_∞ . Surface plots correspond to successive times from 0 to T_{cl} . Vertical axes show z , horizontal axes show ρ .

Putting $n_0 = n_{eff}$, $d\Delta(n_0)/dn \approx 0$, and using (17), we obtain $T_{rev} \approx 30 T_{cl}$.

As a further illustration of the temporal dynamics of a packet, Fig. 6 shows a plot of $\langle t|z^2|t\rangle/z_i^2$ over a long evolutionary time span ($z_i = 2n_{eff}^2$ is the classical turning point for the trajectory I_∞). During the first hundred classical oscillations, we can clearly make out a sequence of wave packet revivals at period T_{rev} , and in between, a set of easily distinguishable oscillations at twice the classical frequency. Gradually, this picture of successive revivals of the packet gets smeared out because of the quadratic anharmonicity, but at times of order $700 T_{cl}$, we again see an unusually clear-cut series of revivals. Moreover, at around $350 T_{cl}$, we observe a sequence of revivals at half the classical period, $T'_{rev} = T_{rev}/2$. Closer inspection reveals that such features can handily be explained in terms of the cubic anharmonicity in Eq. (16). Leaving aside a detailed analysis, we merely note

that in complete analogy with our examination of quadratic anharmonicity, we can determine the period of the cubic anharmonicity to be

$$T_{rev}^{(3)} \approx \pi/3 \gamma. \quad (20)$$

Thus, this period turns out to be one-sixth what one might expect from trivially requiring cancellation of the cubic contribution via

$$\gamma t \approx 2\pi. \quad (21)$$

At $t \approx T_{rev}^{(3)} \approx m T_{rev}$, with m an integer, the cubic contribution leads to recovery of the original wave packet shifted in time by $T_{cl}/6 + (m/2)T_{cl}$:

$$|t\rangle \approx |t + \frac{T_{cl}}{6} + \frac{m}{2} T_{cl}\rangle_{in}, \quad (22)$$

and we see a clear-cut sequence of revived wave packets. Curiously enough, if we can neglect higher-order terms

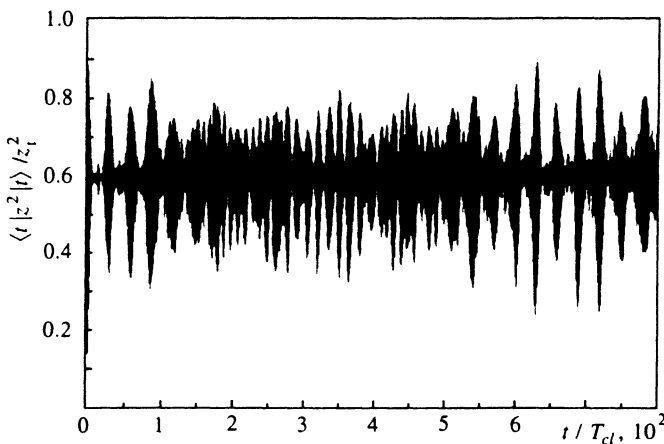


FIG. 6. Time dependence of $\langle t|z^2|t\rangle/z_i^2$ for $K = 19$, $\varepsilon = -0.5$, $z_i = 2n_{eff}^2$ is the classical turning point for the trajectory I_∞ .

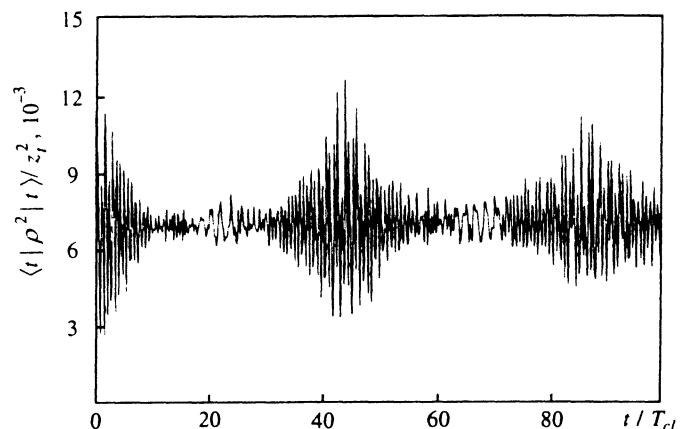


FIG. 7. Time dependence of $\langle t|\rho^2|t\rangle/z_i^2$ for $K = 19$, $\varepsilon = -0.5$.

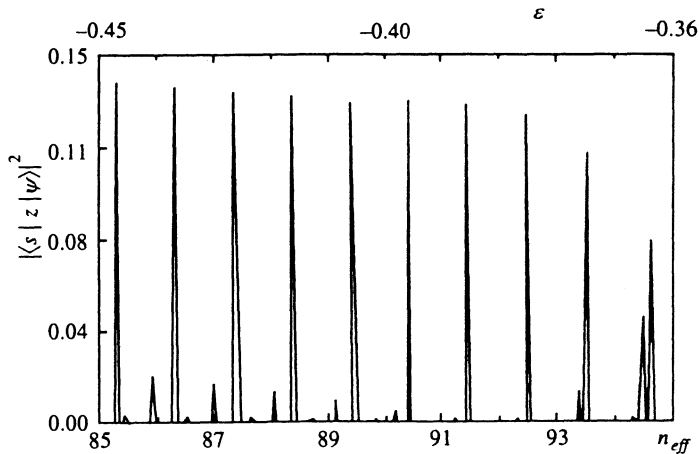


FIG. 8. Spectrum of oscillator strengths, $K=19$, $\varepsilon=-0.4$.

(quartic, etc.), the revived wave packets at time $T_{\text{rev}}^{(3)}$ turn out to be even better defined than the first set of recurrences produced by the quadratic anharmonicity.

We can characterize the feature of the temporal evolution at $t \approx 350T_{cl}$, by analogy with the quadratic anharmonic case, as a fractional revival associated with the cubic anharmonicity. Recall that in the case of quadratic anharmonicity, the fractional revival of order $1/2$ corresponds to splitting of the wave packet into two parts of equal amplitude, shifted by $T_{cl}/2$ and moving in antiphase.³ This corresponds to the onset of oscillations at twice the classical frequency during wave-packet evolution. For the case of cubic anharmonicity, the evolution at time $T_{\text{rev}}^{(3)}/2 \approx mT_{\text{rev}} + T_{\text{rev}}/4$ corresponds to division of the wave packet into two similar but unequal parts that also move in antiphase.

Finally, we present a plot of the temporal evolution of $\langle t|\rho^2|t\rangle/z_t^2$ (see Fig. 7). As expected, the amplitude of the oscillations in the radial direction ρ is almost two orders of magnitude smaller than that in the z direction. The oscillations occur at the Coulomb period T_{cl} , which is the same as the period of trajectory I_∞ . At the same time, the period of wave-packet revivals is associated with the anharmonicity in the energy differences between the main sequence and the first subordinate subsequence in the oscillator-strength plot of Fig. 2.

Yet another example of excitation of the orbit I_∞ is provided by the case with $\varepsilon \approx -0.4$, in which the orbit winds up

in the bifurcation region. The oscillator-strength plot is shown in Fig. 8. The elements of the main sequence form a ‘‘Coulomb’’ series, and are related in a natural way to the states most strongly localized along the field. The oscillator strengths corresponding to these states vary smoothly as the bifurcation region is traversed, decreasing abruptly upon emergence into the region of greatest instability of the orbit I_∞ , where multiplets appear in the spectrum at the location of isolated lines; these multiplets result from interference between the various classical trajectories. In the bifurcation region, series corresponding to satellite subsequences have essentially vanished. The nature of this behavior becomes transparent when we analyze the semiclassical expression (7) for the oscillator strength. At the instant of bifurcation, $M_{12} \rightarrow 0$, and the conventional semiclassical expansion goes to infinity, signifying the fact that the contribution of the given orbit has become anomalously large.

Features in the oscillator-strength spectrum show up in the evolution of the correlation function and packet means. Fig. 9 shows the time dependence of the correlation function. The outstanding feature here is the faithfulness with which the wave packet has been recovered: $\max|\langle 0|t\rangle| \approx 0.9$. Fig. 10 shows the evolution of the ρ^2 , which is characterized by a lack of any evidence for wave-packet revival, and by a reduction in the amplitude of oscillations relative to the case with $\varepsilon \approx -0.5$.

In studying the evolution of z^2 shown in Fig. 11, we

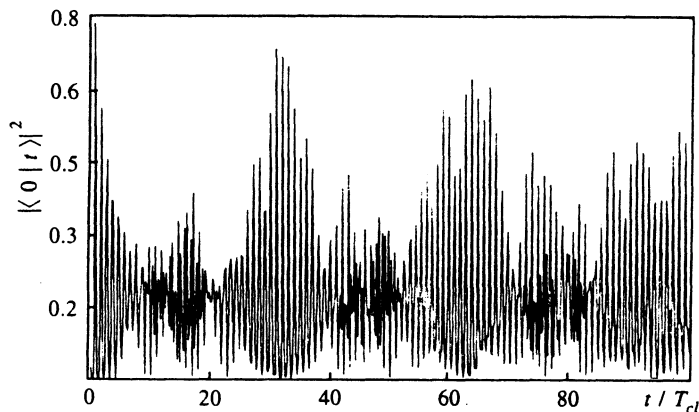


FIG. 9. Time dependence of the correlation function; $K=19$, $\varepsilon=-0.4$.

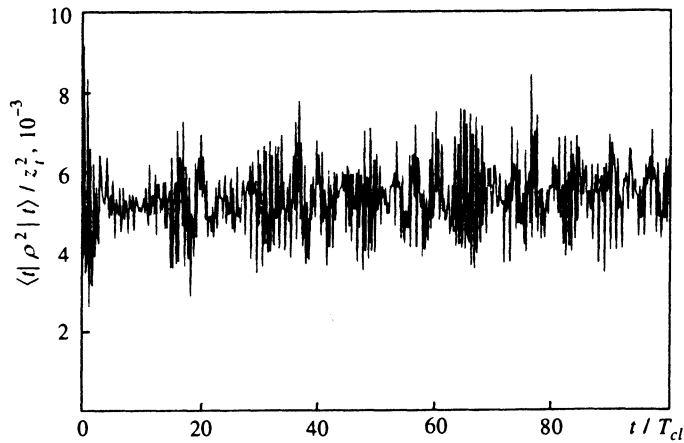


FIG. 10. Time dependence of $\langle | \rho^2 | t \rangle / z_t^2$ for $K=19$, $\varepsilon=-0.4$.

again note the well-defined revival of the wave packet at times $t \approx 1100 T_{cl}$. An analysis shows that this feature results from the cubic anharmonicity in the following way. Let δ be the coefficient of the quartic anharmonicity in Eq. (16); we can then define a new period related to the quartic term:

$$T_{\text{rev}}^{(4)} = \pi/6\delta. \quad (23)$$

At time $t \approx T_{\text{rev}}^{(4)} \approx kT_{\text{rev}}^{(3)} \approx (m + \frac{5}{6})T_{\text{rev}}$, (m and k are integers), the combined contribution of the quartic, cubic, and quadratic anharmonicity lead to a revival of the wave packet.

3.2. Excitation of the orbit I_2

We now consider the excitation of the geometrically nontrivial closed orbit I_2 (Fig. 12). The most favorable conditions for selectively exciting this orbit occur at $\varepsilon \approx -0.32$, where the contribution of the orbit I_∞ is strongly suppressed. At this value of ε , the initial polar angle of the I_2 trajectory is $\theta_{I_2} = 25.12^\circ$, which is almost identical to the classical angle of maximum deviation of the semimajor axis $\theta_0 = 25.04^\circ$ for a vibrational diamagnetic state with $K=15$.

Figure 1 shows the quantum mechanical angular distribution function (8), which peaks near θ_0 . The oscillator-

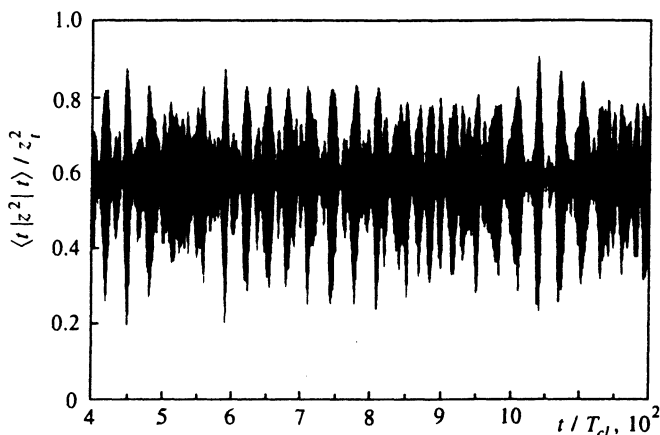


FIG. 11. Time dependence of $\langle | z^2 | t \rangle / z_t^2$ for $K=19$, $\varepsilon=-0.4$.

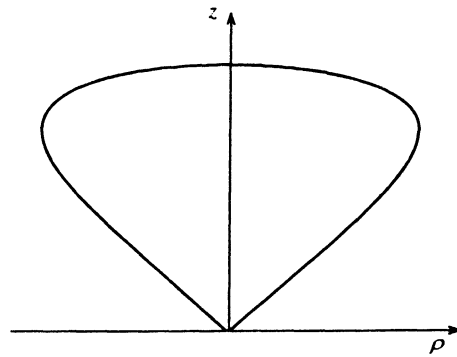


FIG. 12. Shape of the classical trajectory I_2 for $\varepsilon=-0.32$.

strength spectrum in Fig. 13 in fact demonstrates the high degree of selectivity in the excitation of states of the irregular spectrum. It can easily be shown that the main sequence in the spectrum of oscillator strengths is directly related to the excitation of states localized along the closed orbit I_2 . To do so, consider the plot of energy differences between neighboring states in the main sequence (Fig. 14). The sequence in question is clearly weakly anharmonic, and the mean energy difference corresponds to the frequency of classical oscillations on trajectory I_2 . The two-dimensional gray-scale images in Fig. 15 illustrate the temporal evolution of the probability density. They are particularly impressive in the present example, and leave no doubt as to the localization of the wave packet along the classical trajectory I_2 .

3.3. Excitation of the orbit I_1

As a final example, we examine the selective excitation of the closed trajectory I_1 for $\varepsilon \approx -0.5$. The diamagnetic state in this calculation is the state with $K=1$, which is localized near $\theta \approx 90^\circ$. Excitation selectivity is somewhat lower in this case (see Fig. 1). As before, however, the main sequence in the spectrum of oscillator strengths in Fig. 16 is uniquely related to the states localized along the trajectory I_1 . An analysis of subordinate sequences in fact leads one to

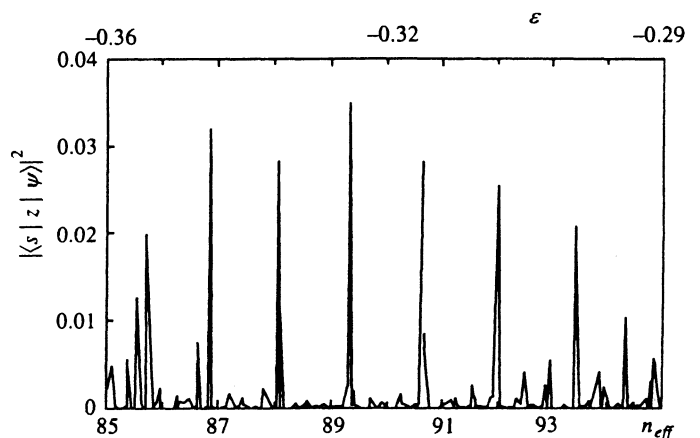


FIG. 13. Spectrum of oscillator strengths, $K=15$, $\varepsilon=-0.32$.

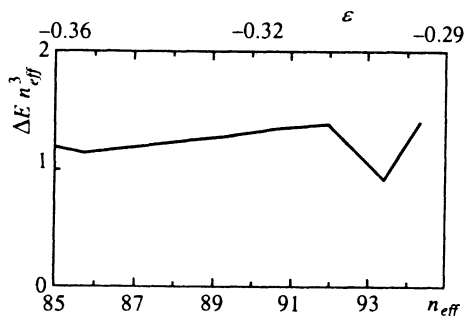


FIG. 14. Energy differences $\Delta E = E_{i+1} - E_i$ between neighboring states of the main sequence in the spectrum of oscillator strengths shown in Fig. 13.

a novel and interesting conclusion about the relationship between features of the classical dynamics and the behavior of irregular quantum spectra.

In studying the evolution of a family of trajectories near I_2 with $\varepsilon = -0.5$, we note that they mimic a certain closed classical trajectory with period $T \approx 3 T_{cl}^1$. For $\varepsilon \approx -0.45$, a new closed classical orbit actually appears with a period that is a multiple of the period of the fundamental classical orbit. Thus, at $\varepsilon \approx -0.5$, we have a resonant or prebifurcation state of the classical system that leads to the emergence of corresponding energy levels in the quantum spectrum.

The evolution of the packet in time is illustrated by the plot of $\langle t | \rho^2 | t \rangle / \rho_i^2$ in Fig. 17. We again see packet revivals in this figure, but they are badly smeared by the fact that a significant fraction of the packet associated with excitation of quiresonant orbits decays rapidly. The evolution of the probability density shown in Fig. 18, bears out the proposition that the packet consists of two differently evolving parts.

4. CONCLUSION

We have examined the excitation of states of the irregular Rydberg spectrum by way of intermediate states of the

regular spectrum. A suitable choice of lower state leads to the isolation of states of the irregular spectrum localized along selected closed classical trajectories, and a substantial simplification of the spectrum of oscillator strengths, thereby making it possible to classify the spectrum in terms of the initial polar angle of the dominant classical orbit. A selective means of excitation results in the generation of wave packets that evolve along specified classical trajectories over the course of hundreds of classical periods. The basic features of the temporal dynamics of various physical quantities can be comfortably explained in terms of the quasi-one-dimensional evolution of a wave packet in a regular spectrum with weak anharmonicity. The natural "one-dimensionalization" factor is the strong localization of the wave packet along the classical trajectory. Analysis of long-term evolution of physical observables yields revival periods linked to higher-order anharmonic corrections to the energy spectrum.

Our work has been supported by the Russian Foundation for Fundamental Research (grant no. 94-02-06022), the International Science Foundation (grant no. R21000), and INTAS. The authors are sincerely grateful to D. Delande for fruitful discussions and for furnishing matrix diagonalization software.

APPENDIX A

To find the discrete spectrum and corresponding eigenfunctions, it is necessary to diagonalize the Hamiltonian matrix (1) in some appropriate basis. The familiar complete basis of hydrogen wave functions contains both a discrete and continuous spectrum, and the latter can make a substantial contribution to the expansion of high-excitation states. In order to avoid any untowardness associated with the continuous spectrum, we can make use of the so-called Sturm basis, which is defined to be the purely discrete complete set of solutions of the equation¹⁵

$$\left(\frac{\mathbf{p}^2}{2} - \frac{Z_n}{r} \right) \Phi_{nlm} = E \Phi_{nlm}, \quad (\text{A1})$$

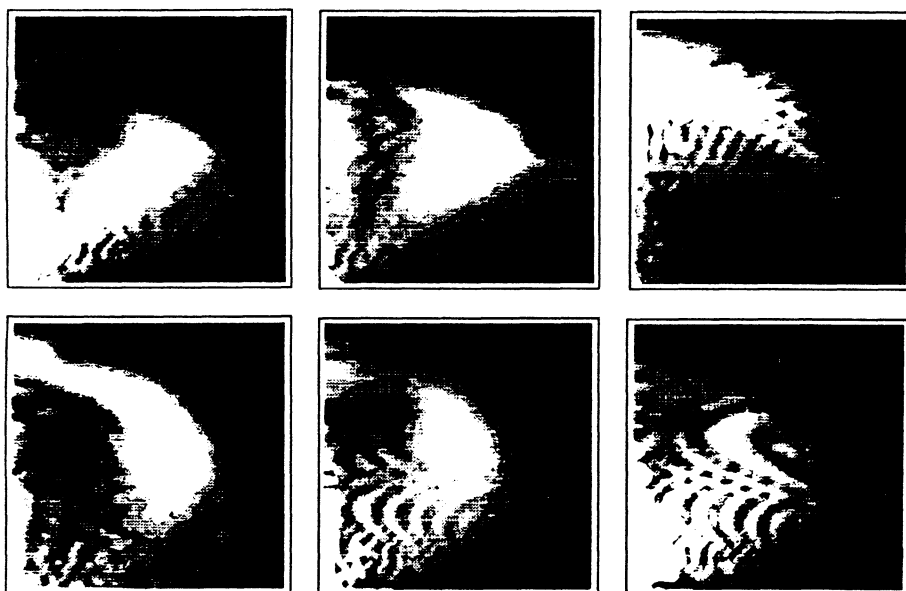


FIG. 15. Evolution of the probability density for a wave packet corresponding to the classical trajectory I_2 . The scale along the ρ (horizontal) axis is three times the scale along the z axis.

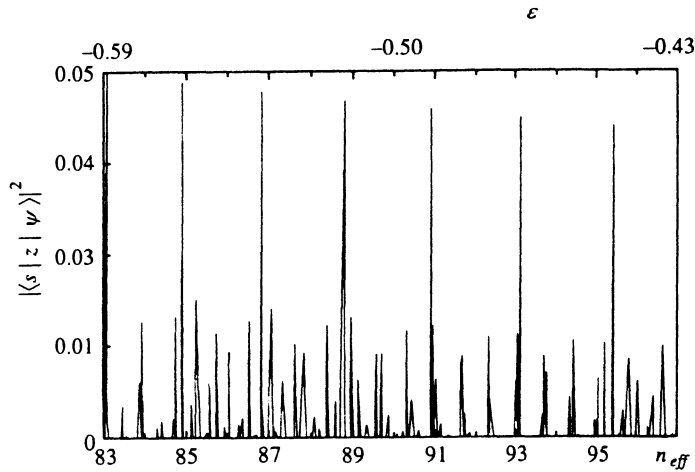


FIG. 16. Spectrum of oscillator strengths, $K=1$, $\varepsilon=-0.5$.

where the energy E is fixed and the charge is quantized: $Z_n = n\sqrt{-2E}$, $n=l+1, \dots, \infty$. The eigenfunctions Φ_{nlm} are orthonormal with weighting factor $1/r$:

$$\left\langle \Phi_{nlm} \left| \frac{1}{r} \right| \Phi_{n'l'm'} \right\rangle = \delta_{nn'} \delta_{ll'} \delta_{mm'}. \quad (\text{A2})$$

In our calculations, the hydrogen-atom wave functions in a magnetic field are given by the expansion

$$|s\rangle = \sum_{l,n} B_{lnm} |\Phi_{nlm}\rangle. \quad (\text{A3})$$

The spectrum of energies E_s and eigenvectors \mathbf{B}^s are obtained by solving the usual matrix problem:

$$\langle \Phi_{nlm} | H - E_s | \Phi_{n'l'm} \rangle B_{nlm}^{(s)} = 0. \quad (\text{A4})$$

We diagonalize the matrix using Lanczos' method. We choose the dimensionality of the basis by requiring that the eigenvalues be calculated to some desired accuracy; in the present case, the dimensionality numbers in the thousands.

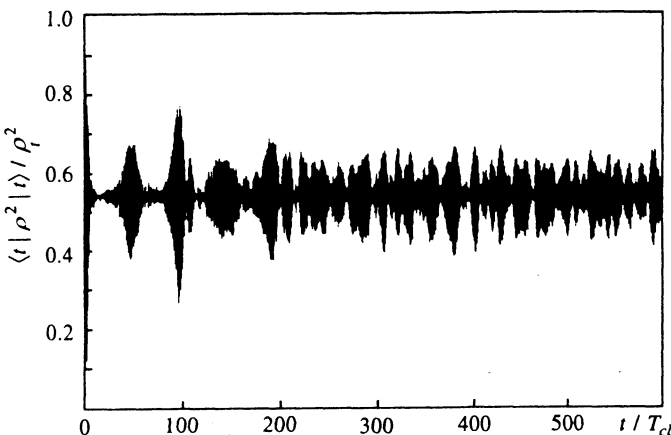


FIG. 17. Time dependence of $\langle t|\rho^2|t\rangle/\rho_0^2$ for $K=1$, $\varepsilon=-0.5$.

APPENDIX B

Following Bogomol'nyĭ,⁷ we give a brief derivation of the semiclassical expression for the spectrum of oscillator strengths (7).

We introduce the Green's function for the standard Schrödinger equation (1):

$$G(x', x; E) = \sum_s \frac{|x, s\rangle \langle x', s|}{E - E_s + i0}, \quad (\text{B1})$$

where E_s and $|x, s\rangle$ are the exact eigenvalues and eigenfunctions of the Schrödinger equation.

Then

$$\text{Im} G(x', x; E) = -\pi \sum_s \delta(E - E_s) |x, s\rangle \langle x', s|, \quad (\text{B2})$$

and the function $f(E)$ of Eq. (6) can be expressed in terms of the Green's function:

$$f(E) = -\frac{1}{\pi} \text{Im} \langle \psi, x | G(x', x; E) | \psi, x' \rangle. \quad (\text{B3})$$

In the semiclassical approximation, the Green's function can be represented as a sum of two terms,

$$G(x', x; E) = G_0(x', x; E) + G^{\text{osc}}(x', x; E), \quad (\text{B4})$$

where $G_0(x', x; E)$ is the contribution made by "short" classical trajectories, whose classical action is small compared with Planck's constant. The semiclassical approximation is inapplicable to such trajectories, but because of their local character, the potential in the Schrödinger equation can be expanded in powers of the deviation from the point $(x' + x)/2$, and in the leading approximation, G_0 is identical with the Green's function in the Thomas-Fermi approximation. In the present problem, G_0 is the pure Coulomb Green's function with no account taken of the external field. The contribution of G_0 to Eq. (B.3) consists of a term $f_0(E)$.

The term $G^{\text{osc}}(x', x; E)$ is the contribution of "long" classical trajectories with large action. In the semiclassical limit, $G^{\text{osc}}(x', x; E)$ can be represented as a sum over all classical trajectories that join x' and x . In n -dimensional space, we have

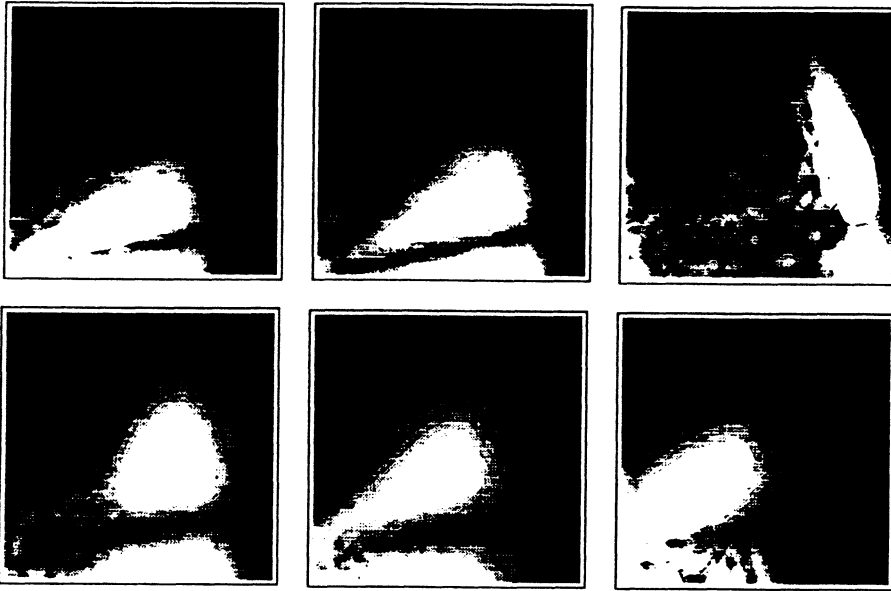


FIG. 18. Evolution of the probability density for a wave packet corresponding to the classical trajectory I_1 .

$$G^{\text{osc}}(x', x; E) = \frac{1}{i\hbar(2\pi i\hbar)^{(n-1)/2}} \sum_{cl} \sqrt{\Delta} \times \exp\left(i \frac{S(x', x; E)}{\hbar} - i\nu \frac{\pi}{2}\right), \quad (\text{B5})$$

where \sum_{cl} is a sum over trajectories, and $S(x', x; E) = \int_x^{x'} \mathbf{p} \cdot d\mathbf{q}$ is the action along a trajectory, with

$$\Delta = \frac{1}{|\dot{\mathbf{q}}'_i| |\dot{\mathbf{q}}_f|} \det\left(\frac{\partial^2 S}{\partial y' \partial y}\right). \quad (\text{B6})$$

Here the y are coordinates in an $(n-1)$ -dimensional plane perpendicular to the current trajectory, $|\dot{\mathbf{q}}|$ is the absolute value of the velocity, and ν is an integer that comes up when there are points on the current trajectory at which the semiclassical approximation breaks down.

The determinant Δ can be conveniently expressed in terms of the elements of the monodromy matrix. Let us fix upon a classical trajectory and write the linearized equations of motion for a nearby family of trajectories:

$$\begin{pmatrix} \dot{y}(t) \\ y(t) \end{pmatrix} = \begin{pmatrix} M_{11}(t) & M_{12}(t) \\ M_{21}(t) & M_{22}(t) \end{pmatrix} \begin{pmatrix} \dot{y}(0) \\ y(0) \end{pmatrix}. \quad (\text{B7})$$

Here we represent the matrix $M(t)$ in block form. If T is the time required to traverse the classical trajectory, then the matrix $M(T)$ is called the monodromy matrix of the given trajectory.

The determinant Δ can easily be rewritten in the form¹⁰

$$\Delta = \frac{1}{|\dot{\mathbf{q}}_i| |\dot{\mathbf{q}}_f| \det[M_{12}(T)]}, \quad (\text{B8})$$

where $|\dot{\mathbf{q}}_i|$ and $|\dot{\mathbf{q}}_f|$ are the initial and final speeds.

For trajectories that do not follow the field, the two-dimensional semiclassical theory holds in cylindrical coordinates z, ρ , and the determinant in Eq. (B.8) reduces to the

matrix element M_{12} . For trajectories linear in the field, $\rho=0$. Writing out the kinetic energy operator in cylindrical coordinates,

$$\mathbf{p}^2 = -\frac{\partial^2}{\partial z^2} - \frac{\partial^2}{\partial \rho^2} + \frac{m^2}{\rho^2},$$

we conclude that the two-dimensional semiclassical model breaks down in this case.

Using the three-dimensional model, according to (B6), if the trajectory runs along the z axis and motion in x is independent of motion in y , then

$$\Delta = \frac{1}{|\dot{\mathbf{q}}'_i| |\dot{\mathbf{q}}_f|} \left(\frac{\partial^2 S}{\partial x' \partial x}\right) \left(\frac{\partial^2 S}{\partial y' \partial y}\right). \quad (\text{B9})$$

As before, each of the second derivatives can be expressed in terms of the corresponding element of the monodromy matrix.

The expression for the oscillator-strength density (B3) contains integrals of the Green's function multiplied by the initial wave function. When the initial state is one with small quantum numbers, the greatest contribution to the integral comes from values of x' and x close to the nucleus. The most important classical trajectories are therefore those that are closed at the nucleus. On the other hand, the simple semiclassical equations do not hold in the immediate vicinity of the Coulomb center, in general, and it is necessary to match a numerical solution to the exact Coulomb functions.

The final semiclassical expression for the density of oscillator strengths looks like

$$f(E) = f_0(E) + f_{\parallel}(E) + f_{\theta}(E). \quad (\text{B10})$$

Here $f_{\parallel}(E)$ is the contribution of the trajectory along the field,

$$f_{\parallel}(E) = N_{\parallel} \sum_j \frac{A^*(0)A(0)}{|M_{12}^{(j)}|} \sin\left(\frac{S_j}{\hbar} - \nu_j \frac{\pi}{2}\right), \quad (\text{B11})$$

$$A(\theta) = \sum_{l'} (-1)^{l'} \langle \psi | z | [n_{\text{eff}}] l' m \rangle Y_{l' m}(\theta, 0), \quad (\text{B12})$$

sums are carried out over all circuits of a trajectory that is linear in the field, and N_{\parallel} is a constant. The contribution $f_{\theta}(E)$ due to all other classical trajectories can be written in similar fashion:

$$f_{\theta}(E) = N_{\theta} \sum_j \frac{A^*(\theta_j^f) A(\theta_j^i)}{\sqrt{|M_{12}^{(j)}|}} \sin\left(\frac{S_j}{\hbar} - \nu_j \frac{\pi}{2}\right), \quad (\text{B13})$$

$$A(\theta) = \sqrt{\sin \theta} \sum_{l'} (-1)^{l'} \langle \psi | z | [n_{\text{eff}}] l' m \rangle Y_{l' m}(\theta, 0), \quad (\text{B14})$$

where summation takes place over all circuits of every classical trajectory.

¹Planck's constant \hbar has been introduced into Eq. (7) as a convenient small formal parameter for semiclassical expansions.

²For a hydrogen atom in a magnetic field, all trajectories that are closed at

the nucleus turn out to be periodic.

¹G. Alber and P. Zoller, Phys. Rep. **199**, 231 (1991).

²A. ten Wolde, L. D. Noordam, H. G. Müller *et al.*, Phys. Rev. Lett. **61**, 2099 (1988).

³I. Sh. Averbukh and N. F. Perelman, Phys. Lett. A **139**, 449 (1989).

⁴P. A. Braun and V. I. Savichev, Phys. Rev. A **49**, 1704 (1994).

⁵P. A. Braun and V. I. Savichev, J. Phys. B: At. Mol. Phys. **26**, 3739 (1993).

⁶M. L. Du and J. B. Delos, Phys. Rev. A **38**, 1896 (1988).

⁷E. B. Bogomol'nyi, Zh. Éksp. Teor. Fiz. **96**, 487 (1989) [Sov. Phys. JETP **69**, 275 (1989)].

⁸N. Bouloufa, P. Cacciani, D. Delande *et al.*, J. de Phys. II (Paris) **2**, 671 (1992).

⁹P. A. Braun and D. Delande, J. Phys. B: At. Mol. Phys. (1995; in press).

¹⁰M. C. Gutzwiller, J. Math. Phys. **B 12**, 343 (1971).

¹¹J. Gao and J. B. Delos, Phys. Rev. A **46**, 1455 (1992).

¹²H. Friedrich and D. Wintgen, Phys. Rep. **183**, 37 (1989).

¹³M. Yu. Sumetskiĭ, Zh. Éksp. Teor. Fiz. **83**, 1661 (1982) [Sov. Phys. JETP **56**, 959 (1982)].

¹⁴A. Holle, J. Main, G. Weibusch, *et al.* Phys. Rev. Lett. **61**, 161 (1988).

¹⁵D. Delande and J. C. Gay, Phys. Rev. Lett. **57**, 2006 (1986).

Translated by Marc Damashek